A Robust Texture Analysis and Classification Approach for Urban Land-Use and Land-Cover Feature Discrimination

Soe Win Myint
Department of Geography
100 East Boyd Street, 684 Sarkeys Energy Center
University of Oklahoma, Norman, OK 73019-1007, U.S.A.
Email: swmyint@ou.edu

Abstract

Attempts to analyze urban features and to classify land use and land cover directly from high-resolution satellite data with traditional computer classification techniques have proven to be inefficient for two primary reasons. First, urban landscapes are composed of complex features. Second, traditional classifiers employ spectral information based on single pixel value and ignore a great amount of spatial information. Texture plays an important role in image segmentation and object recognition, as well as in interpretation of images in a variety of applications. This study analyzes urban texture features in multi-spectral image data. Recent developments in the very powerful mathematical theory of wavelet transforms have received overwhelming attention by image analysts. An evaluation of the ability of wavelet transform in urban feature extraction and classification was performed in this study, with six types of urban land cover features classified. The preliminary results of this research indicate that the accuracy of texture analysis in classifying urban features in fine resolution image data could be significantly improved with the use of wavelet transform approach.

Introduction

While remote sensing technology has been applied successfully in many areas, especially in natural resource assessment and monitoring, the results reported for urban environments have generally been much less satisfactory (Barnsley *et al*., 1989; Corners *et al*., 1984; Forster, 1985; Jensen and Toll, 1982; Moller-Jensen, 1990; Sadler and Barnsley, 1990; Toll, 1984). The fundamental problem usually found in identifying urban land cover types from high-resolution satellite imagery is that urban areas are composed of diverse materials (metal, glass, concrete, asphalt, plastic, shingles, water, grass, shrubs, trees, soil, etc.). These materials, each of which may have completely different spectral characteristics, are combined in complex ways by human beings. Hence, each urban land cover type may contain several different objects with different reflectance values. Noisy appearance with lots of edges, and the complex nature of these images, inhibit accurate interpretation of urban features.

As the spatial resolution of the sensor increases, individual scene elements (buildings, roads, trees, grassland, water, parks, sidewalk, bare soil, etc.) begin to dominate the detected response of each pixel; therefore, the spectral response of urban areas as a whole becomes more varied, making classification of urban areas more difficult (Gastellu-Etchegorry, 1990). Unfortunately, traditional spectral classification algorithms are inefficient to handle this type of spatial variability because they assign each pixel to one of the categories on the basis of its spectral reflectance properties or its individual pixel value and ignore huge amount of information on the spatial arrangements of neighboring pixels (Barnsley and Baar, 1992; Barnsley *et al*., 1991; Woodcock and Strahler, 1987).

Another problem for supervised classification is that it is extremely difficult to define suitable training sets for many categories within urban environments. This is due to variation in the spectral response of their component land cover types (Barnsley *et al*., 1991; Foster, 1985; Gong and Howarth, 1990). Thus, the training statistics may exhibit very high standard deviations (Sadler *et al*., 1991) and violate one of the basic assumptions of the widely used maximum-likelyhood decision rule, namely that the pixel values follow a multivariate normal distribution (Barnsley *et al*., 1991; Sadler *et al*., 1991). Various attempts have been made to overcome these problems.

Texture

Texture plays an important role in the human visual system for pattern recognition and interpretation. Texture is the visual impression of coarseness or smoothness caused by

the variability or uniformity of image tone or color (Avery and Berlin, 1992). It is the most widely used definition of texture in pattern recognition and image classification but it does not reflect the complete description and characterization of a texture.

Although it is quite easy for human observers to recognize and describe in empirical terms, texture has been extremely refractory to precise definition and to analysis by digital computers (Haralick *et al*., 1973). Some of the terms used to describe textures have ambiguous physical meanings. For example, does 'coarse' texture mean that the overall variability of pixel value is large or that pixels tend to occur in large, contrasting blocks or both? (Lark, 1996).

Texture is an elusive notion which mathematicians and scientists tend to avoid because they cannot grasp it. Engineers and artists cannot avoid it, but mostly fail to handle it to their satisfaction (Mandelbrot, 1983). Lark (1996) described a working definition of texture as follows. Two segments of an imagery may be regarded as having the same texture if they do not differ significantly with respect to: (i) the variance of their DN values, (ii) the spatial dependence of this variability at a characteristic scale (or scales), (iii) the directional dependence of this variability, and (iv) any spatial periodicity of this variation. This working definition does not claim to be comprehensive but it is proposed as a useful basis for image analysis in the context of remote sensing (Lark, 1996).

There is no universally accepted mathematical definition of texture. The general approach is to develop a symbolic representation for texture and determine computer methods for associating images of texture patterns with their symbolic descriptions, though at the present time there does not exist a commonly accepted set of descriptive terms for texture. Some descriptive terms that could be applied to explain texture patterns in different ways may include fine and coarse, directionality (orientation), smooth and rough, random and deterministic, regular and irregular, linear and non linear, high and low density, phases, and high and low frequency.

Texture Analysis

There have been some attempts to improve the spectral analysis of remotely sensed data by using texture transforms in which some measure of variability in DN values is estimated within local windows, e.g., contrast between neighboring pixels (Edwards *et al*., 1988), standard deviation (Arai 1993), or local variance (Woodcock and Harward, 1992). In the past, texture has been shown to be useful in suburban fringe of urban areas (Conners *et al*., 1984; Moller-Jensen, 1990). The coefficient of variance gives a measure of the total relative variation of pixel values in an area and can be computed easily, but it gives no information about spatial patterns (De Jong and Burrough, 1995). Burrough (1993), Klinkenberg (1992), and Snow and Mayer (1992) criticized many other neighborhood operations such as diversity or variation filters.

Despite the lack of a neat and complete characterization of fractals (Mandelbrot, 1987), many studies have used fractal geometry as a basis to quantify previously intractable natural patterns (Roach and Fung, 1994). Although several studies attempted to use different fractal algorithms: isarithm, triangular prism, and variogram (Clarke, 1986;. Lam and De Cola, 1993; Mark and Aronson, 1984; Quattrochi *et al*., 1997) to characterize texture features in remote sensing applications (De Cola, 1989; De Jong and Burrough, 1995; Emerson *et al*., 1999; Jaggi *et al*., 1993; Kaplan, 1999; Lam, 1990; Lam and Quatrochi, 1992; Lam *et al*., 1998; Qiu *et al*., 1999; Roach and Fung, 1994), evidence suggests that there are a number of limitations in using such techniques to characterize texture and identify land use and land cover classes (Burrough, 1989; 1993; Clarke and Schweizer, 1991; De Jong and Burrough, 1995; Dong, 2000; Goodchild and Mark, 1987; Klinkenberg and Goodchild, 1992; Mandelbrot, 1983; Mandelbrot,1995; Mark and Aronson, 1984; Myint, 2001; Peleg, *et al*., 1984; Pentland, 1984; Roach and Fung, 1994; Voss, 1986; Xia, 1993).

There have been some experiments to extract texture features with spatial co-occurrence matrix or gray level spatial dependency in a moving window to show the relationship between a given pixel and its specified neighbor (Conners and Harlow, 1980; Franklin *et al*., 2000; Franklin and Pedddle, 1987; Franklin and Pedddle, 1989; Hall and Fent, 1996; Haralick, 1979; Haralick *et al*., 1973; Moller-Jensen, 1990; Pedddle and Franklin, 1990; Pedddle and Franklin, 1991; Pesaresi, 2000; Sali and Wolfson, 1992; Wulder, *et al*., 1996). The spatial co-occurrence matrix is a widely used texture and pattern recognition technique in the analysis of remotely sensed data, and it has been successful to a certain extent. However, it focuses primarily on the coupling between image pixels on a single scale and a single band, and it may not discriminate between closely related urban features. This is also true for spatial autocorrelation techniques, as they all focus on a single scale and single band. An additional problem is the choice of displacement vector $v = (\Delta x, \Delta y)$, because the co-occurrence matrix characterizes the spatial relationship between pixels for a given vector.

The new spatial/frequency analysis tools, such as Gabor transform, Wigner distribution, discrete cosine transform, and wavelet transforms (Bovik and Clark, 1990; Turner, 1986; Yang and Chen, 1994), are considered good multi-resolution analysis tools. Particularly, wavelet transforms play an important role in texture analysis and classification (Zhu and Yang, 1998). This study explores the use of wavelet transforms in the analysis of high-resolution remotely sensed data.

Recent studies using wavelet transforms for texture analysis have generally reported better accuracy. Carter (1991) reported 98% accuracy in the classification of six types of natural textures. Chang *et al*. (1993) examined classification of images from Brodatz's album (1966) and achieved 99.6% accuracy. However, none of these researchers applied wavelet decomposition technique to texture features in remotely sensed images. Zhu and Yang (1998) classified

25 types of geomorphologic features or terrain patterns in images with an accuracy as high as 100%. Sheikholeslami *et al*. (1999) demonstrated a multi-resolution wavelet-based approach for geographic images with very high rate of retrieval.

Wavelet Theory Basics and Analysis

Wavelet theory is the mathematics associated with building a model for a signal, system, or process with a set of "special signals." The special signals are just little waves or "wavelets" They must be ocscillatory (waves) and have amplitudes that quickly decay to zero in both the positive and negative directions (Young, 1998).

In wavelet theory, the scaling and translation operators act simultaneously on the mother wavelet function. The name "wavelet", literally meaning "little wave", originated from the study of Grossmann and Morlet (1984). The mother wavelet (the initial little wave) is the kernel of the wavelet transform. Performing affine operations on the mother wavelet creates a set of scaled and translated versions of this mother wavelet function. The general form of wavelet transform of a one-dimension signal can be defined as (Daubechies, 1992).

$$Wf\,(\mathrm{a},\,\mathrm{b}) = \int_{-\mathrm{a}}^{+a} f\,(x)\psi_{a,b}\,(x)\,dx \qquad (1)$$

$$\psi_{a,b}\,(x) = \frac{1}{\sqrt{|a|}}\psi\left(\frac{x-b}{a}\right),\ (a,b \in R, \mathrm{a} \neq 0) \qquad (2)$$

which is translated and scaled versions of a function ψ, in which the wavelet function ψ is dilated by a factor a and shifted by b. The function ψ is called a mother wavelet. An integral transformation using the functions above as a basis is called a wavelet transformation. For digital signals, a discrete wavelet ψ— which is formed from ψ by sampling the parameters a and b following the Nyquist theorem — is used (Grossman and Morlet, 1984). Multiplying each wavelet coefficient by the appropriately scaled and shifted wavelet yields the constituent wavelets of the original signal. Wavelets are well-located in both domains: space and scale (Daubechies, 1990).

The decomposition process can be iterated, with successive transformed signals being decomposed. In wavelet analysis, a signal is split into an approximation and a detail. The approximation is then itself split into a second level approximation and detail, and the process is repeated. This is a standard procedure of wavelet decomposition, called the wavelet decomposition tree (figure 1). In theory the analysis process can be iterated indefinitely. In the real world situation, the decomposition can proceed only until the individual details consist of a single sample or pixel.

Multiresolution Wavelet Decomposition

Mallat (1989 a and b) developed the multiresolution analysis theory using the orthonormal wavelet basis. A wavelet is orthogonal when all of the pairs formed from the basis functions $\psi_{j,k}$ are orthogonal to each other. An orthogonal wavelet which norm is normalized to one is called an orthonormal wavelet (Fukuda and Hirosawa, 1989). The multiresolution wavelet transform decomposes a signal into low frequency approximation and high frequency detail information at coarser resolution. In satellite image analysis using 2-D wavelet transform techniques, rows and columns of image pixels are considered signals.

The approximation and details of a two-dimensional image $f(x,y)$ at resolution 2^j can be defined by the coefficients computed by the following convolutions:

$$A^{d}_{2^j} f = ((\, f(x,y) * \varnothing_{2^j}(-x)\varnothing_{2^j}(-y))\,(2^{-j}n, 2^{-j}m))_{(n,m)\in Z^2} \qquad (3)$$

$$D^{1}_{2^j} f = ((\, f(x,y) * \varnothing_{2^j}(-x)\psi_{2^j}(-y))\,(2^{-j}n, 2^{-j}m))_{(n,m)\in Z^2} \qquad (4)$$

$$D^{2}_{2^j} f = ((\, f(x,y) * \psi_{2^j}(-x)\varnothing_{2^j}(-y))\,(2^{-j}n, 2^{-j}m))_{(n,m)\in Z^2} \qquad (5)$$

$$D^{3}_{2^j} f = ((\, f(x,y) * \psi_{2^j}(-x)\psi_{2^j}(-y))\,(2^{-j}n, 2^{-j}m))_{(n,m)\in Z^2} \qquad (6)$$

where integer j is a decomposition level, m, n are integers, $\varnothing(x)$ is a one-dimensional scaling function, and $\psi(x)$ is a one-dimensional wavelet function. In general, $\varnothing(x)$ is a smoothing function which provides low frequency information, and $\psi(x)$ is a differencing function which provides high frequency information. $A^{d}_{2^{j+1}} f$ can be perfectly reconstructed from $A^{d}_{2^j} f$, $D^{1}_{2^j} f$, $D^{2}_{2^j} f$, $D^{3}_{2^j} f$.

The expressions (3) through (5) show that in two dimensions, $A^{d}_{2^j} f$, $D^{k}_{2^j} f$ are computed with separable filtering of the signal along the abscissa and ordinate. The wavelet decomposition can thus be interpreted as a signal decomposition in a set of independent, spatially oriented frequency channels (Mallat, 1989a).

We need a filter bank (a set of filters) to perform multiresolution wavelet decomposition. Filter banks used for signal analysis are commonly composed of lowpass and highpass filters. They separate the input signal into frequency bands in a process referred to as subband coding. Filters are linear time-invariant operators that act on input vectors x to generate output vectors y. In this case, y is the convoluted version of x with a fixed vector h. In discrete time $t = nT$, the input $x(n)$ and output $y(n)$ will appear at all times t = -3, -2, -1, 0, 1, 2....

There is a scaling function $\varnothing(x)$ related to the lowpass filter, and a wavelet function $\psi(x)$ related to the highpass filter. They can be defined as:

$$\text{Dilation equation } \varnothing(t) = \sqrt{2}\sum_k c(k)\varnothing(2t-k) \qquad (7)$$

$$\text{Wavelet equation } \psi(t) = \sqrt{2}\sum_k d(k)\varnothing(2t-k) \qquad (8)$$

For example, Haar, the simplest wavelet transform, has coefficients: $c(0) = c(1) = 1/\sqrt{2}$, $d(0) = 1/\sqrt{2}$, and $d(1) = -1/\sqrt{2}$. Thus, its dilation equation and wavelet equation can be expressed as:

$$\phi t=\phi(2t)+\phi(2t\text{-}1) \quad (9)$$

$$\psi t=\phi(2t)+\phi(2t\text{-}1) \quad (10)$$

The approximation and detail coefficients can be computed with a pyramid algorithm based on convolutions with the above mentioned two one-dimensional parameter filters. Approximation of a signal $A^{d}_{2^j} f$, also known as trend, can be obtained by convolving the input signal $A^{d}_{2^{j+1}} f$, with the lowpass filter (*Lo_F*). First, the rows of an image are convolved with one-dimensional *Lo_F*. Next, the filtered signals are down sampled. In the first step, down sampling is performed by keeping one column out of two. Then the resulting signals are convolved with another one-dimensional lowpass filter, retaining every other row. To obtain a horizontal detail image, first the rows of the input image are convolved with a lowpass filter *Lo_F*, and the filtered signals are down sampled by keeping one column out of two, as we do in processing approximation images. However, for the next stage, the columns of the signals are convolved with a highpass filter *Hi_F*, and again every other row is retained. For the vertical details, the original signals are convolved first with a highpass filter *Hi_F* and then with a lowpass filter *Lo_F*, following the above procedure. For the diagonal detail image, the same down sampling procedure is carried out, using two highpass filters consecutively. The algorithm for the application of the filters and down sampling procedure for computing the approximation and details coefficients is illustrated in figure 2. It shows in the frequency domain how the image $A^{d}_{2^{j+1}} f$ is decomposed into $A^{d}_{2^j} f$, $D^{1}_{2^j} f$, $D^{2}_{2^j} f$ and $D^{3}_{2^j} f$ sub-images. The sub-image $A^{d}_{2^j} f$ corresponds to the lowest frequencies (approximation), $D^{1}_{2^j} f$ gives the vertical high frequencies (horizontal edges), $D^{2}_{2^j} f$ the horizontal high frequencies (vertical edges), and $D^{3}_{2^j} f$ the high frequency in both directions (the diagonal edges).

Figure 3 represents a standard orthonormal wavelet decomposition with 2 levels of an image. This is again illustrated by the decomposition of a randomly selected training sample of a residential area generated from ATLAS remotely sensed data. The pyramid decomposition can be continuously applied to the approximation image until the desired coarser resolution 2^{-j} ($-1 \geq j \geq -J$) is reached.

Let us suppose that initially we have an image $A_1 f$ measured at resolution 1. For any $J > 0$, this discrete image can be decomposed between resolutions 1 and 2^{-j}, and completely represented by the $3J + 1$ discrete images.

$$(A^{d}_{2^{-j}} f, (D^{1}_{2^j} f)_{-J \leq j \leq -1}, (D^{2}_{2^j} f)_{-J \leq j \leq -1}, (D^{3}_{2^j} f)_{-J \leq j \leq -1}).$$

This set of images is called an orthogonal wavelet representation in two dimensions. If the original image has N pixels, each sub-image $A^{d}_{2^j} f$, $D^{1}_{2^j} f$, $D^{2}_{2^j} f$, $D^{3}_{2^j} f$ will have $2^j N$ pixels ($j < 0$). The total number of pixels in this new representation is equal to the number of pixels of the original image. This is due to the orthogonality of the representation (Mallat, 1989 a, b).

Data, Study Area, and Sampling Design

Advanced Thermal Land Application Sensor (ATLAS) image data at 2.5 m spatial resolution acquired with 15 channels (0.45 μm - 12.2 μm) was used for this research. The data was collected by a NASA Stennis LearJet 23 flying at 6600 feet over Baton Rouge, Louisiana, on May 7, 1999.

In this research experiment, six urban land-cover features with different textural appearances were selected. The selected land-cover classes include single-family homes with less than 50% tree canopy (residential-1), single-family homes with more than 50% tree canopy (residential-2), commercial, woodland, agriculture, and water body. Two segmented regions of each land-cover class were visually identified with the help of local area knowledge, ground information collection, and existing maps. Five training pixels were then randomly selected from each region leading to a sample of 10 pixels. In this study, a 65x65 square window size centered at the randomly selected pixels in each region was used to subset training samples. Criteria for the selection of window size were image resolution, minimum mapping unit size,

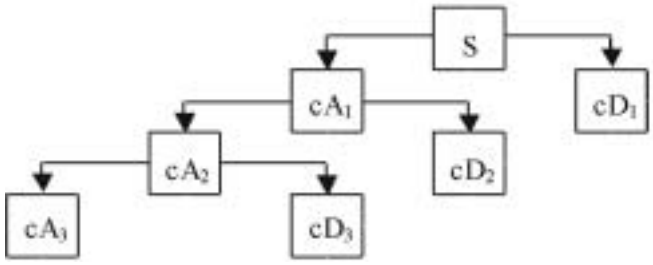

S = signal; cA = approximation; cD = details.

Figure 1 A signal's wavelet decomposition tree

Figure 2 Decomposition of an image $A^{d}_{2^{j+1}} f$ into $A^{d}_{2^j} f$ (approximation), $D^{1}_{2^j} f$(horizontal details), $D^{2}_{2^j} f$ (vertical details), and $D^{3}_{2^j} f$ (diagonal details).

and the nature of the classes (size of the regions, characteristic scale, orientation of features, and spatial periodicity) to be identified. It is understood that smaller window size does not cover sufficient spatial/texture information to characterize land cover types. However, if the window size is too large, too much information from other land-use types could be included and hence the algorithm might not be efficient. The samples were generated from approximately 900 columns by 7800 rows of one of the seven flight lines available over Baton Rouge area.

It was observed that textures of the same area in different bands (e.g., visible, reflected infrared, and thermal infrared) were different in terms of contrast, smoothness and coarseness, directionality, and spatial variation. Since different texture appearances of the same area in different band were observed, four different bands were selected and examined in this study. Band-2 (0.52-0.60 (m) was selected as it represents a visible band. Band-6 (0.76-0.90 (m) was selected to represent a near infrared band, and band-12 (9.60-10.20 (m) represents a thermal band. Figure 4 shows the differences in texture features of the same area in three different bands in the Baton Rouge ATLAS image: band-2, band-6 and band-12. In addition to the above, principal component analysis (PCA), a technique that compresses redundant data and produces bands that are often more interpretable than the original data, was applied to all available bands in the ATLAS data. PCA-1 band was selected and examined in this study since it includes the largest percentage of the total scene variance. The succeeding components (PCA2, PCA3, PCA4, etc,) each contains a decreasing percentage of the scene variance were excluded in this study since they contain noise and represent only a little information on texture features of land cover classes. Thus, the complete data set consists of 240 unique samples (10 samples per class x 6 classes x 4 bands). Samples of the classes are shown in figure 5.

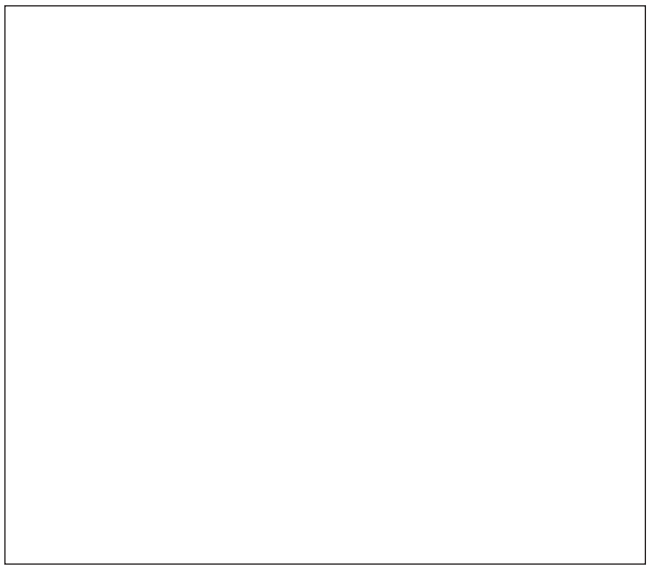

Figure 3 A standard orthonormal wavelet decomposition with 2 levels of a sample image (residential area)

Texture Measure

Haralick *et al*. (1973) proposed a variety of measures to extract textural information from the gray level cooccurrence matrices (GLCM), also known as the spatial cooccurrence matrix. GLCM is the most widely used method in characterizing textures in image analysis (Barber and Ledrew, 1991; Berry and Goutsias, 1991; Carstensen, 1992; Conners and Harlow, 1980; du Buf *et al*., 1990; Franklin and Peddle, 1987; Franklin and Peddle, 1989; Franklin and Peddle, 1990; Haralic *et al*., 1973; Jensen, 1979; Jensen, 1982; Peddle and Franklin, 1991; Pesaresi, 2000; Sali and Wolfson, 1992; Siew *et al*., 1988; Vickers and Modestino, 1982; Weszka *et al*., 1976; Wulder *et al*., 1996). In general, the texture measures in GLCM include contrast, homogeneity, angular second moment, inverse different moment, and entropy. Gong and Howarth (1992) demonstrated the efficiency of occurrence frequency methods with the use of several measures: mean, standard deviation, skewness, kurtosis, range, and entropy measures. Zhu and Yang (1998) used information entropy as a measure to identify texture features in twenty-five types of aerial relief samples selected from remote sensing images. Albuz *et al*. (1999) used the sum of squares of the wavelet coefficients of each sub-band for their image retrieval system. Sheikholeslami *et al*. (1999) calculated the mean and variance of wavelet coefficients to represent the contrast of the image. In this study, four feature measures: log energy (*LOG*), shannon's index (*SHAN*),

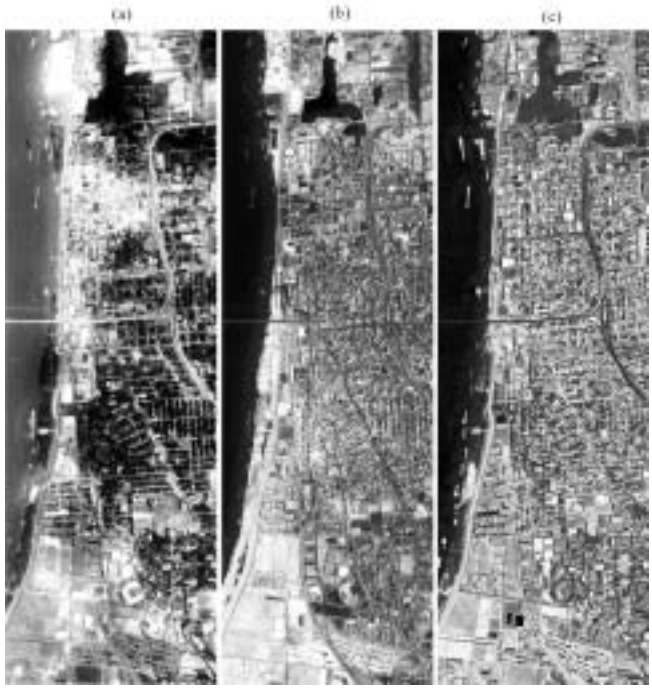

Figure 4 A subset of the southern part of the Baton Rouge metropolitan area (southeast of Louisiana State University in the lower left part of the photo) is shown in three separate bands: (a) band 2 (0.52-0.93 μm: visible green), (b) band 6 (0.76-0.93 μm: reflected infrared), and (c) band 12 (9.00-9.40 μm: thermal infrared)

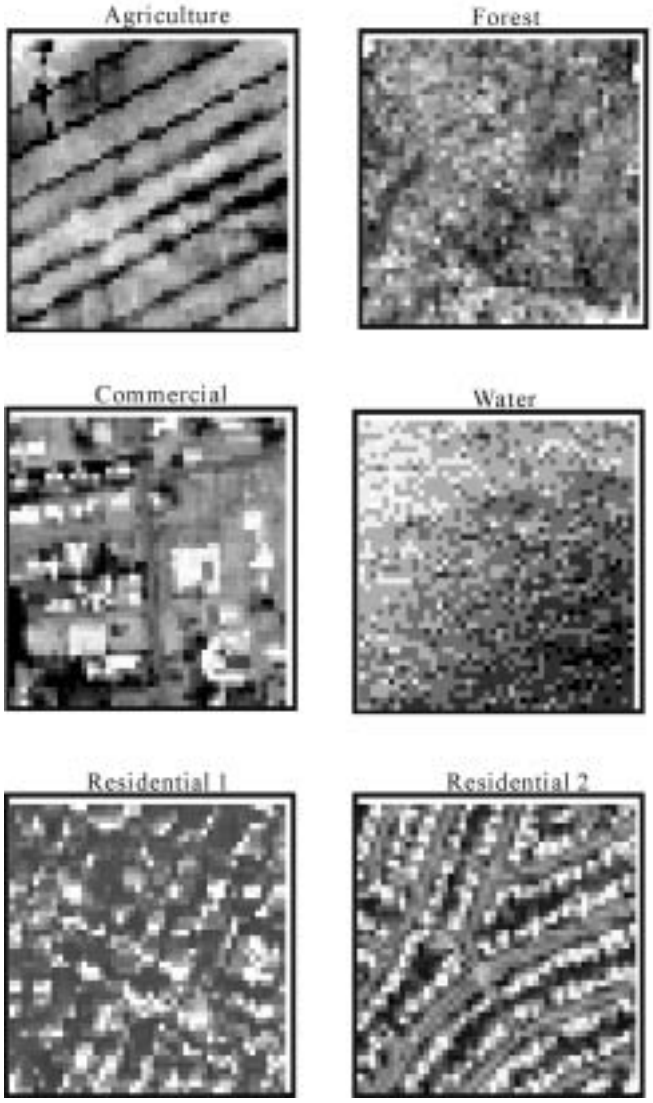

Figure 5 Samples of six urban texture features

entropy (*ENT*), and angular second moment (*ASM*) were used to characterize the texture of urban land-use and land-cover classes

$$LOG = \sum_{i=1}^{k}\sum_{j=1}^{k}\log(P(i,j)^2) \quad (11)$$

$$SHAN = \sum_{i=1}^{k}\sum_{j=1}^{k}P(i,j)*\log(P(i,j)) \quad (12)$$

$$ASM = \sum_{i=1}^{k}\sum_{j=1}^{k}P(i,j)^2 \quad (13)$$

$$ENT = \sum_{i=1}^{k}\sum_{j=1}^{k}Q(i,j)*\log|Q(i,j)|; \quad Q(i,j)= \frac{|P(i,j)|^2}{\sqrt{\sum_{i,j}|P(i,j)|^2}} \quad (14)$$

where $P(i,j)$ is the (i,j)th pixel wavelet coefficient value of a decomposed image at a particular level. A program using MATLAB software package was developed by the author to perform wavelet decompositions and to compute above mentioned texture measures in the analysis.

Classification

To evaluate the efficiency of the wavelet transform technique for texture classification, linear discriminant analysis approach was used. The texture measures (e.g., entropy of the decomposed sub-images) for the sample generated above were subject to discriminant analysis. This is useful for situations in which we want to build a predictive model of group membership based on the observed characteristics of each case. Minitab software package was used to perform discriminant analysis for the classification of land cover features in this study. The procedure generates a discriminant function (or, for more than two groups, a set of discriminant functions) based on linear combinations of the predictor variables, which provide the best discrimination between the groups. The discriminant analysis was carried out to discriminate between textural features of urban land use and land cover on the basis of the texture measure value of the wavelet coefficients of sub-images at different levels. For example, the entropy values of the wavelet coefficients at different levels for the four different bands (visible, near infrared, thermal, and PCA1) were treated as variables to identify features of urban land-use and land-cover classes. The Discriminant analysis was chosen as the method of implementing a classification because it has been shown to be less sensitive to the number of mapping variables and less affected by deviations from the normal (Gaussian) distribution compared to other classification techniques such as maximum likelihood (Tom and Miller, 1984). It is also important to note that classification accuracy is in part a function of the class structure used with respect to the spatial and radiometric precision of the data (Hutchinson, 1982).

Generally, further decomposition is performed in the low frequency channels, and this is known as the standard wavelet decomposition approach. Using the standard decomposition procedure, linear discriminant analysis was performed for six types of 65x65 texture samples generated from band-2, band-6, band-12, and PCA1 band. Error matrices were later generated for all separate levels and combinations of different levels for all measures: *LOG*, *SHAN*, *ENT*, and *ASM*. Wavelet decomposition was performed up to 4 levels with 65x65 samples. The decomposition levels are denoted by l_1, l_2, l_3, and l_4 in the classification.

Result and Discussion

It is apparent from the results for all bands and all measures that overall accuracy decreases with increasing resolution. In other words, the lower the level of sub-images we use to compute texture measures for classification, the lower the accuracy we obtain. The results may be due to the size of lower-level sub-images, which cover less spatial frequency information since they are just a quarter each of their mother

body. Mother body is referred to as the original image used for further decomposition. It could be either the original image or any one of the sub-images: approximation, horizontal, vertical, and diagonal details before decomposition. If the original image has N pixels, each sub-image $A_{2^j}^d f, D_{2^j}^1 f, D_{2^j}^2 f, D_{2^j}^3 f$, will have $2^j N$ pixels ($j < 0$) at jth level.

The accuracy trend by level of decomposition found in this contribution is similar to the human detection accuracy curve demonstrated by Hodgson (1998) and the empirical general histogram distance index reported by Pesaresi (2000). They both generally demonstrate that classification accuracy increases with increasing window size. It should be noted that the overall accuracy obtained from a sub-image at a lower level may be slightly higher than its mother body in some exceptional cases. However, in most cases, the accuracy of lower-level sub-images exceeded that of higher-level sub-images. We can also draw a general conclusion for all bands that the overall accuracy for the combination of different levels is much higher than for any single level alone. It was also found that the combination of a greater number of levels yielded much higher accuracy than combination of a lesser number of levels. The results were not normally degraded when using more levels. It can generally be concluded that the larger the number of levels of combination, the higher the accuracy. This result may be due to more spatial and frequency information captured by a texture measure when using a combination of more levels. It is obvious that the combination of more levels provides more spatial frequency information. Hence, the highest accuracy found in the overall classifications was produced by the combination of l_1, l_2, l_3, and l_4. However, it is important to note that sub-images very close to the end stage (the lowest level) may not provide much spatial/frequency information. Hence, sub-images at extremely low levels may not improve the existing accuracy or may even lead to poorer accuracy in some cases.

Because the first level produced the highest accuracy among all single levels and the combination of the maximum number of levels yielded the highest accuracy among all different combinations, I present in this paper the different accuracy rates for each category only at the

Table 1 Overall classification accuracy, producer's/user's accuracies of different urban land-use and land-cover classes using level 1

Band	Classes	Texture Measures											
		LOG			SHAN			ENT			ASM		
		P_{ACC} (%)	U_{ACC} (%)	O_{ACC} (%)	P_{ACC} (%)	U_{ACC} (%)	O_{ACC} (%)	P_{ACC} (%)	U_{ACC} (%)	O_{ACC} (%)	P_{ACC} (%)	U_{ACC} (%)	O_{ACC} (%)
Band-2	A	40	100		70	78		80	89		70	78	
	C	90	100		70	78		70	88		70	78	
	F	80	57		90	90		100	91		90	90	
	L	80	80		90	90		80	73		90	90	
	M	80	62		100	77		100	91		100	77	
	W	70	70		80	89		100	100		80	89	
				73			83			88			83
Band 6	A	70	70		70	70		80	73		70	78	
	C	50	63		50	63		40	67		60	67	
	F	80	89		100	100		90	100		100	100	
	L	80	80		70	78		70	70		70	78	
	M	100	77		80	62		90	64		80	62	
	W	100	100		100	100		100	100		100	100	
				80			78			78			80
Band-12	A	80	73		80	62		80	67		80	67	
	C	30	75		40	57		50	63		60	67	
	F	100	91		100	100		80	100		100	100	
	L	90	64		100	91		100	83		100	100	
	M	100	100		90	100		90	90		90	100	
	W	100	100		100	100		100	100		100	100	
				83			85			83			88
PCA1	A	50	71		90	90		80	100		90	90	
	C	70	78		70	88		70	78		70	88	
	F	90	90		100	100		100	100		100	100	
	L	90	75		100	77		100	83		100	77	
	M	90	75		90	100		90	82		90	100	
	W	100	100		100	100		100	100		100	100	
				82			92			90			92

P_{ACC} = producer's accuracy; U_{ACC} = user's accuracy; O_{ACC} = overall accuracy

Table 2 Overall classification accuracy, producer's/user's accuracies of different urban land-use and land-cover classes using combination of 4 levels

Band	Classes	Texture Measures											
		LOG			SHAN			ENT			ASM		
		P_{ACC} (%)	U_{ACC} (%)	O_{ACC} (%)	P_{ACC} (%)	U_{ACC} (%)	O_{ACC} (%)	P_{ACC} (%)	U_{ACC} (%)	O_{ACC} (%)	P_{ACC} (%)	U_{ACC} (%)	O_{ACC} (%)
Band-2	A	90	90		90	100		90	100		100	100	
	C	90	100		90	82		100	91		90	100	
	F	90	100		100	100		100	91		100	100	
	L	100	100		90	100		90	100		100	100	
	M	100	91		100	91		100	100		100	91	
	W	70	70		80	89		100	100		80	89	
				95			95			97			98
Band 6	A	90	100		100	100		100	100		100	100	
	C	100	91		100	100		100	100		100	100	
	F	100	100		100	100		100	100		100	100	
	L	100	100		100	100		100	100		100	100	
	M	100	100		100	100		100	100		100	100	
	W	100	100		100	100		100	100		100	100	
				80			78			78			80
Band-12	A	90	100		100	71		100	100		100	83	
	C	100	91		50	100		100	91		70	100	
	F	100	100		100	100		100	100		100	100	
	L	100	100		100	91		100	100		100	91	
	M	100	100		100	100		90	100		100	100	
	W	100	100		100	100		100	100		100	100	
				98			92			98			95
PCA1	A	100	91		80	89		100	100		80	89	
	C	80	89		80	73		100	100		80	73	
	F	100	100		100	100		100	100		100	100	
	L	90	90		90	90		100	91		90	90	
	M	100	100		100	100		90	100		100	100	
	W	100	100		100	100		100	100		100	100	
				95			92			98			92

P_{ACC} = producer's accuracy; U_{ACC} = user's accuracy; O_{ACC} = overall accuracy

first level and the combination of 4 levels in terms of overall accuracy, producer's accuracy (P_{Acc}), and user's accuracy (U_{Acc}) in table 1 and 2 respectively. It can be observed that there is some confusion among agriculture, commercial, and residential-1 classes. Texture features of residential-2 generated from band-6 also produced relatively low user's and producer's accuracy. It seems that there is also some confusion between residential-1 and residential-2 generated from band-6. In fact, they both are closely related or similar texture features. It was unexpectedly found that most of the measures in this study were very efficient in discriminating between these two closely related texture features. The only highly reliable category associated with this classification technique is water body. It reaches the highest user's and producer's accuracies (100%) for all bands and almost all measures. This is probably due to its smooth nature of texture compared to other land cover features. It normally does not have edges, directionality, spatial periodicity, (Lark, 1996) and characteristic scale, whereas the rest of the texture features possess complex appearances with pronounced anisotropy and spatial periodicity. However, almost all categories reach 100% user's and producer's accuracy for almost all measures for all bands.

The highest accuracies at the first level produced for band-2, band-6, band-12, and PCA1 were found to be 88%, 80%, 88%, and 92% respectively. It is noted that there is no huge difference of classification accuracies among all bands when using the combination of all 4 levels. The highest accuracies using the combination of 4 levels yielded by band-2, band-12, band-6, and PCA1 were 98%, 98%, 100%, and 98% respectively. Although band-6 produced the lowest accuracies for almost all measures at the first level, it achieved the highest accuracies after combining all 4 levels. The overall classification accuracies yielded by the combination of 4 levels for all 4 bands exceed the minimum mapping accuracy level of 85% (Townshend, 1981) required for most resource management and applications.

Conclusion and Future Research

A trend is evident from figure 6 (a), (b), (c), and (d) that overall accuracy decreases with increasing resolution for all bands and all measures. In general, the combination of all 4

levels produced the highest accuracy. Table 3 shows the overall classification accuracy achieved at each level and combination of different levels for each band and each measure. Generally, *ENT* shows highest performances in three bands; band-6, band-12, and PCA1. It was originally thought that *ENT* would consistently characterize the textures of urban areas more efficiently than the others since it is based on the probability of each wavelet coefficient in a window. What has been observed is that other texture measures, in certain situations, can produce a slightly higher accuracy than that of *ENT* measure. However, it can be noted that there is no significant difference of accuracies among all measures. From the above findings, we can draw a general conclusion that all measures used in this study are fairly equally efficient.

Band-6 seems to be the most efficient band in characterizing textures in urban land-cover features, since samples of band-6 with the combination of four levels using *SHAN* or *ENT* or *ASM* measure reaches an overall accuracy as high as 100%. The reasons for obtaining the highest accuracy may be the combination of two effects: the measures and the wavelet transforms. The measures used here in the study could effectively grasp the details in noise and describe information related properties for an accurate representation of a given signal (rows or columns). More importantly wavelet representation of a feature provides details or edges of textures in horizontal, vertical, and diagonal orientations and approximation or smoothing effect of the original signal at multiple scale. In other words, wavelet provides four different texture features at each scale in the multiresolution analysis. Future research is required to develop a procedure to select optimal window size. However, this may depend on the nature of the study area, data resolution, classification specificity, and characteristics of texture features. A number of smaller local window sizes needs to be evaluated for the same classes since larger window sizes tend to cover more land cover features and consequently lead to poorer accuracy. It is important to note that samples used in this study were randomly selected from homogeneous texture features and a sample having 2 or more land cover features were not considered. The results in this study do not reflect the boundary effect problems, which are common in the real world. Hence it

Table 3 Overall classification accuracies for all 4 bands

			Overall accuray(%) (Measures)			
Band	L	NSI	LOG	SHAN	ENT	ASM
Band-2 (visible)	l_1	4	73.3	83.3	88.3	83.3
	l_2	4	65.0	81.7	80.0	85.0
	l_3	4	68.3	63.3	60.0	66.7
	l_4	4	58.3	58.3	58.3	60.0
	l_1-l_2	8	90.0	91.7	88.3	91.7
	l_1-l_3	12	93.3	93.3	91.7	91.7
	l_1-l_4	16	95.0	95.0	96.7	98.3
Band-6 (near infrared)	l_1	4	80.0	78.3	78.3	80.0
	l_2	4	76.7	83.3	80.0	83.3
	l_3	4	80.0	83.3	80.0	81.7
	l_4	4	56.7	56.7	53.3	58.3
	l_1-l_2	8	91.7	88.3	93.3	88.3
	l_1-l_3	12	93.3	95.0	96.7	96.7
	l_1-l_4	16	98.3	100.0	100.0	100.0
Band-12 (thermal)	l_1	4	83.3	85.0	83.3	88.3
	l_2	4	68.3	85.0	76.7	86.7
	l_3	4	61.7	68.3	73.3	66.7
	l_4	4	56.7	53.3	56.7	55.0
	l_1-l_2	8	88.3	83.3	88.3	85.0
	l_1-l_3	12	93.3	91.7	93.3	91.7
	l_1-l_4	16	98.3	91.7	98.3	95.0
PCA1	l_1	4	81.7	91.7	90.0	91.7
	l_2	4	70.0	86.7	85.0	86.7
	l_3	4	61.7	60.0	65.0	58.3
	l_4	4	50.0	53.3	58.3	50.0
	l_1-l_2	8	88.3	88.3	95.0	88.3
	l_1-l_3	12	96.7	91.7	98.3	91.7
	l_1-l_4	16	95.0	91.7	98.3	91.7

L = wavelet decomposition level; NSI = number of sub-images

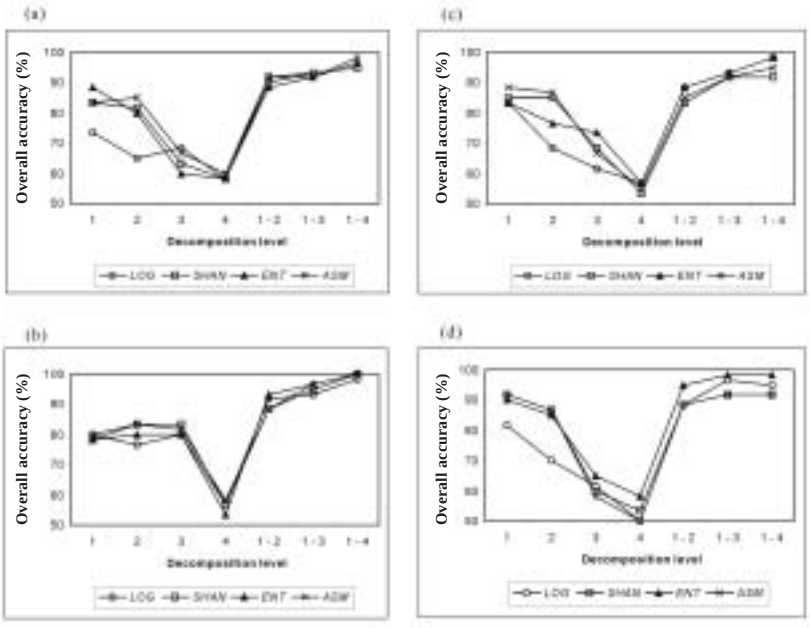

Figure 6 (a), (b), (c), (d) Overall accuracy for LOG, SHAN, ENT, and ASM plotted against separate decomposition level and combination of different levels using standard decomposition approach for band-2, band-6, band-12, and PCA1 band respectively

is also recommended that mixed boundary features or problem areas be included in future research.

There is also a question of other candidates that could provide better accuracy than the texture measures employed in this study. The preliminary results of this research indicated that the accuracy of texture analysis in classifying fine resolution image data could be significantly improved with the use of the wavelet transforms approach. The potential of the methods for wavelet analysis proposed in this study needs to be tested in other environments. It is recommended that the other wavelet transform techniques be examined since Haar wavelet is the simplest and oldest approach among all wavelet transforms.

Acknowledgements

This research was supported by the Otis Paul Starkey Fund (The Association of American Geographers) under the AAG grants/awards and the Robert C. West field research grant (Department of Geography and Anthropology, LSU). The author thanks John Tyler, Dept. of Computer Science, LSU and Nina Lam, Dept. of Geography and Anthropology, LSU for their suggestions during the analytical phases of this research. The author also expresses his appreciation to DeWitt Braud, Dept. of Geography and Anthropology, LSU for providing the ATLAS data for this study.

References

Albuz, Elif, E. Kocalar, A.A. Khokhar, 1999. Vector-wavelet based scalable indexing and retrieval system for large color image archives, *IEEE Transactions on Geoscience and Remote Sensing*, 44:3021-3024.

Barber, D.G., and E.F. LeDrew, 1991. Sar Sea Ice Discrimination Using Texture Statistics: A Multivariate Approach, *Photogrammetric Engineering and Remote Sensing*, 57(4):385-395.

Barnsley, M.J., S.L. Barr, and G.J. Sadler, 1991. Spatial re-classification of remotely sensed images for urban land-use monitoring, *Proceedings of Spatial Data 2000*, Oxford, 17-20 September, Remote Sensing Society, Nottingham, pp. 106-117.

Barnsley, M.J., G.J. Sadler, and J.S. Shepherd, 1989. Integrating remotely sensed images and digital map data in the context of urban planning. *Proceedings of the 15th Annual Conference of the Remote Sensing Society*, Bristol, U.K., 13-15 September, Remote Sensing Society, Nottingham, pp. 25-32.

Barnsley, M.J., and S.L. Barr, 1992. Developing kernel based spatial re-classification techniques for improved land-use monitoring using high spatial resolution images, *Proc. XXIX Conference of the International Society for Photogrammetry and Remote Sensing(ISPRS' 92). International Archives of Photogrammetry and Remote Sensing: Commission 7*, Washington D.C., 2-14 August 1992, pp. 646-654.

Berry, L.R. and Goutsias, J., 1991. A comparative study of matrix measures for maximum likelihood texture classification. *IEEE Transactions on Systems, Man, and Cybernetics*, 21(1): 252-261.

Bovik, A.C., and M. Clark, 1990. Multichannel texture analysis using localized spatial filters, *IEEE Transactions on Pattern Analysis and Machine Intelligence*, 12:55-73.

Brodatz, P., 1966. *Textures*: A photographic album for artists & designers, New York: Dover, New York.

Burrough, P.A., 1989. Fractal and Geochemistry, The Fractal Approach to Heterogeneous Chemistry (D. Avnir, editor), Wiley & Sons Ltd., pp. 383-405.

————, 1993. Soil Variability: A Late 20th Century View, *Soils and Fertilizers*, pp. 529-562.

Carstensen, J.M., 1992. *Description and Simulation of Visual Texture*, Ph.D. Thesis, Technical University of Denmark, 225 p.

Carter, P.H., 1991. Texture discrimination using wavelet, In *SPIN application of digital image processing* XIV, 1567:132-438.

Chang, T., and C.-C.J. Kuo, 1993. Texture analysis and classification with tree-structured wavelet transform, *IEEE Transactions on Image Processing*, 2(4):429-441.

Clarke, K.C., 1986. Computation of the Fractal Dimension of Topographic Surfaces Using the Triangular Prism Surface Area Method, *Computers and Geosciences*, 12(5):713-722.

Clarke, K.C., and D.M. Schweizer, 1991. Measuring the Fractal Dimension of Natural Surfaces Using a Robust Fractal Estimator, *Cartography and Geographic Information Systems*, 18(1):37-47.

Conners, R.W., and C. Harlow, 1980. A theoretical comparison of texture algorithms, *IEEE Transactions on Pattern Analysis and Machine Intelligence*, 2(3):204-222.

Conners, R.W., M. Trivedi, and C. Harlow, 1984. Segmentation of a High-Resolution Urban Scene Using Texture Operators, *Computer Vision, Graphics, and Image Processing*, 25:273-310.

Daubechies, I., 1990. The wavelet transform, time/frequency localization and signal analysis, *IEEE Trans. Inform. Theory*, 36:961-1005.

Daubechies, I., 1992. Ten lectures on wavelets, *CBMS-NSF Regional Conference Series on Applied Mathematics*, Vol. 61, Society for Industrial and Applied Mathematics, Philadelphia, PA, USA.

De Cola, L. (1989). Fractal Analysis of a classified Landsat scene, *Photogrammetric Engineering and Remote Sensing*, 55:601-610.

De Jong, S.M., and P.A. Burrough, 1995. A Fractal Approach to the classification of Mediterranean Vegetation Types in Remotely Sensed Images, *Photogrammetric Engineering and Remote Sensing*, 61:1041-1053.

Dong, P., 2000. Lacunarity for Spatial Heterogeneity Measurement in GIS, Geographic Infromation Sciences, 6(1):20-26.

du Buf, J.M.H., M. Kardan, and M. Spann, 1990. Texture feature performance for image segmentation. *Pattern Recognition*, 23(3):291-309.

Edwards, G., R. Landary, and K.P.B. Thomson, 1988. Texture analysis of forest regeneration sites in high-resolution SAR imagery, *Proceedings of the International Geosciences and Remote Sensing Symposium* (IGARSS 88), ESA SP-284 (Paris: European Space Agency), pp 1355-1360.

Emerson, C.W., N.S.N. Lam, and D.A. Quattrochi, 1999. Multi-Scale Fractal Analysis of Image Texture and Pattern, *Photogrammetric Engineering and Remote Sensing*, 65(1):51-61.

Foster, B.C., 1985. An examination of some problems and solutions in monitoring urban areas from satellite platforms, *International Journal of Remote Sensing*, 6:139-151.

Franklin, S.E., and D. Peddle, 1987. Texture analysis of digital image data using spatial cooccurrence, *Computer & geosciences*, 13(3):293-311.

Franklin, S.E., and D. Peddle, 1989. Spectral texture for improved class discrimination in complex terrain, *International Journal of Remote Sensing*, 10:1437-1443.

Franklin, S.E., and D. Peddle, 1990. Classification of SPOT HRV imagery and texture features, *International Journal of Remote Sensing*, 11:551-556.

Franklin, S.E., R.J. Hall, L.M. Moskal, A.J. Maudie, and M.B. Lavigne, 2000. Incorporating texture into classification of forest species composition from airborne multispectral images, *International Journal of Remote Sensing*, 21(1):61-79.

Fukuda, S., and H. Hirosawa, 1998. Suppression of speckle in synthetic aperture radar images using wavelet. *International Journal of Remote Sensing*, 19(3):507-519.

Gastellu-Etchegorry, J.P., 1990. An assessment of SPOT XS and Landsat MSS data for digital classification of near-urban land cover, *International Journal of Remote Sensing*, 11:551-556.

Gong P. and Howarth, P.J., 1990. The use of structural information for improving land cover classification accuracies at the rural urban fringe, *Photogrammetric Engineering and Remote Sensing*, 56(1):67-73.

————, 1992. Frequency based contextual classification and gray level vector reduction for land use identification, *Photogrammetric Engineering and Remote Sensing*, 58(4):423-437.

Goodchild, M.F., and D.M. Mark, 1987. The Fractal Nature of Geographic Phenomena. *Annals of the Association of American Geographers*, 77(2):265-278.

Grossmann, A., and Morlet, J., 1984. Decomposition of Hardy functions into square integrable wavelets of constant shape, *SIAM Journal on Mathematical Analysis* 15:723-736.

Hall, R.J., and L. Fent, 1996. Influence of aerial film spectral sensitivity and texture on interpreting images of forest species composition, *Canadian Journal of Remote Sensing*, 22(4):350-359.

Haralick, R.M., 1979. Statistical and structural approaches to texture, *Proceedings of the I.E.E.E.*, 67, 786-804.

Haralick, R.M., K. Shanmugan, and J. Dinstein, 1973. Textural features for image clasification, *IEEE Transaction on Systems, Man, and Cybernetics*, SMC-3(6):610-621.

Hodgson, M.E., 1998. What size window for image classification? A cognitive perspective, *Photogrammetric Engineering and Remote Sensing*, 64(8):797-807.

Hutchinson, C.F., 1982. Techniques for Combining Landsat and Ancillary Data for Digital Classification Improvement. *Photogrammetric Engineering and Remote Sensing*, 48(1):123-130.

Jaggi, S., D.A. Quattrochi, and N.S.N. Lam, 1993. Implementation and operation of three fractal measurement algorithms for analysis of remote-sensing data, *Computer and Geosciiences*, 19(6):745-767.

Jensen, J.R., 1979. Spectral and textural features to classify elusive land cover at the urban fringe, *Professional Geographer*, 31:400-409.

————, 1982. Detecting residential land-use development at the urban fringe *Photogrammetric Engineering and Remote Sensing*, 48:629643.

Jensen, J.R., and D. Toll, 1982. Detecting residential land use development at the rural-urban fringe, *Photogrammetric Engineering and Remote Sensing*, 48: 629-643.

Kaplan, L.M., 1999. Extended fractal Analysis for texture classification and segmentation. *IEEE Transactions on Image Processing*, 8:1527-1585.

Klinkenberg, B., 1992. Fractals and Morphometric Measures: Is there a Relationship?, *Geomorphology*, 5:5-20.

Klinkenberg, B. and M.F. Goodchild, 1992. The Fractal Properties of Topography: A Comparison of Methods, *Earth Surface Processes and Landforms*, 17:217-234.

Lam, N.S.N., 1990. Description and Measurement of Landsat TM Images Using Fractals, *Photogrammetric Engineering and Remote Sensing*, 56(2):187-195.

Lam, N.S.N., and D.A. Quattrochi, 1992. On the Issues of Scale, Resolution, and Fractal Analysis in the Mapping Sciences, *Professional Geographer*, 44(1):88-97.

Lam, N.S.N., and L. De Cola, 1993. Fractal Simulation and Interpolation, *Fractals in Geography* (N.S.N. Lam and L. De Cola, editors), Prentice Hall, Englewood Cliffs, New Jersey, pp. 56-74.

Lam, N.S.N, D. Quattrochi, H. Qui, and W. Zhao, 1998. Environmental assessment and monitoring with image characterization and modeling system using multiscale remote sensing data, *Applied Geographic Studies*, 2(2): 77-93.

Lark, R.M., 1996. Geostatistical description of texture on an aerial photograph for discriminating classes of land cover, *International Journal of Remote Sensing*, 17: 2115-2133.

Mark, D.M., and P.B. Aronson, 1984. Scale Dependent Fractal Dimensions of Topographic Surfaces: An Empirical Investigation with Applications in Geomorphology and Computer Mapping, *Mathematical Geology*, 16:671-683.

Mandelbrot, B.B., 1983. *The Fractal Geogetry of Nature*. New York: Freeman and Co.

Mandelbrot, B.B., 1987. "Fractals," *Encyclopedia of Physical Science and Technology*, Vol. 5, pp. 579-593.

Mandelbrot, B. (1995). Measures of Fractal Lacunarity: Minkowski Content and Alternatives, *Progress in Probability*, 37:15-42.

Mark, D.M., and P.B. Aronson, 1984. Scale Dependent Fractal Dimensions of Topographic Surfaces: An Empirical Investigation with Applications in Geomorphology and Computer Mapping, *Mathematical Geology*, 16:671-683.

Moller-Jensen, L., 1990. Knowledge-based classification of an urban area using texture and context information in Landsat-TM imagery, *Photogrammetric Engineering and Remote Sensing*, 56(6):899-904.

Peddle D.R. and S.E. Franklin, 1990. GEDEMON: A Fortran-77 Program for Restoration and Derivative Processing of Digital Image Data. *Computers and Geosciences*, 16(5):669-696.

Peddle D.R. and S.E. Franklin, 1991. Image Texture Processing and Data Integration for Surface Pattern Discrimination, *Photogrammetric Engineering and Remote Sensing*, 57:413-420.

Peleg, S., Noar, J., Hartley, R., and Avnir, D, D., 1984, Multiple resolution texture analysis and classfication, *IEEE Transactions on Pattern Analysis and Machine Intelligence*, PAMI-6(4):518-528.

Pentland, A., 1984. Fractal-based description of natural scenes, *IEEE Transactions on Pattern Analysis and Machine Intelligence, PAMI-*6(6):661-674.'

Pesaresi, M., 2000. Texture Analysis for Urban Pattern Recognition Using Fine-resolution Panchromatic Satellite Imagery, *Geographical and Environmental Modelling*, 4(1):43-63.

Quattrochi, D.A., N.S.N. Lam, H. Qiu, and W. Zhao, 1997. Image Characterization and Modeling System (ICAMS): A Geographic Information System for the Characterization and Modeling of Multiscale Remote Sensing Data, *Scale in Remote Sensing and GIS* (D.A. Quattrochi and M.F. Goodchild, editors), CRC Press, Boca Raton, Florida, pp. 295-308.

Qiu, H, N.S. Lam, D.A. Quattrochi, and J.A. Gamon, 1999. Fractal Characterization of Hyperspectral Imagery, *Photogrammetric Engineering and Remote Sensing*, 65(1) :63-71.

Roach, D., and K.B. Fung, 1994. Fractal-based textural descriptors for remotely sensed forestry data, *Caanadian Journal of Remote Sensing*, 20:59-70.

Sadler, G.J., M.J. Barnsley, 1990. Use of population density data to improve classification accuracies in remotely sensed images of urban areas. *Proceedings of the First European Conference on Geographical Information Systems (EGIS'90)*, Amsterdam, The Netherlands, 10-13 April, EGIS foundation, Utrecht, pp. 968-977.

Sadler, G.J., M.J. Barnsley, and S.L. Barr, 1991. Information extraction from remotely-sensed images for urban land analysis, *Proceedings of the Second European Conference on Geographical Information Systems (EGIS'91)*, Brussels, Belgium, April, EGIS Foundation, Utrecht, pp. 955-964.

Sali, E., and Wolfson, H., 1992. Texture classification of Arid geomorphic surfaces using Landsat spectral and textural features, *International Journal of Remote Sensing*, 13:3395-3408.

Sheikholeslami, G., A. Zhang, and L. Bian, 1999. A Multi-Resolution Content-Based Retrieval Approach for Geographic Images, *Geoinformatica*, 3(2):109-139.

Siew, L.H., R.M. Hodgson, and E.J. Wood, 1988. Texture measures for carpet wear assessment. *IEEE Transactions on Pattern Analysis and Machine Intelligence*, 10(1):92-105.

Snow, R.S., and L. Mayer, 1992. Fractals in *Geomorphology*, Geomorphology, 5(1/2):194.

Toll, D.L., 1984. An evaluation of simulated Thematic Mapper data and Landsat MSS data for determining suburban and regional land use and land cover. *Photogrammetric Engineering and Remote Sensing*, 50(12):1713-1724.

Tom, C.H., and L.D. Miller, 1984. An automated land-use Mapping Comparison of the Bayesian Maximum Likelihood and Linear Discriminant Analysis Algorithms. *Photogrammetric Engineering and Remote Sensing*, 50(2):193-207.

Townshend, J.R.G., 1981. *Terrain Analysis and Remote Sensing*. George Allen and Unwin: London, 272 p.

Turner, M.R., 1986. Texture transformation by Gabor function, *Biology Cybernation*, 55:71-82.

Vickers, A.L., and J.W. Modestino, 1982. A maximum likelihood approach to texture measures for terrain classification. *IEEE Transactions on Pattern Analysis and Machine Intelligence*, 4(1):61-68.

Voss, R., 1986. Random Fractals: characterization and measurement, *Scaling Phenomena in Disordered Systems*, Pynn, R. and Skjeltorp, A. eds., Plenum, New York.

Weszka, J.S., C.R. Dyer, and A. Rosenfeld, 1976. A comparative study of texture classification. *IEEE Transactions on Pattern Analysis and Machine Intelligence*, 4(1), 61-68.

Woodcock, C.E., and A.H. Strahler, 1987. The factor of scale in remote sensing, *Remote Sensing of Environment*, 21:311-332.

Woodcock, C., and V.J. Harward, 1992. Nested-hierarchical scene models and image segmentation, *International Journal of Remote Sensing*, 13:3167-3187.

Wulder, M.A., S.E. Franklin, and M.B. Lavigne, 1996. High spatial resolution optimal image texture for improved estimation of forest stand leaf area index, *Canadian Journal of Remote Sensing*, 22(4):441-449.

Xia, Z., 1993. *The Uses and Limitations of Fractal Geometry in Digital Terrain Modelling*, Ph.D. Thesis, City University of New York, 252 p.

Young, R.K., 1998. *Wavelet Theory and Its Applications*, Kluwer Academic Publishers, sixth edition, 1998, Massachusetts, 223 p.

Zhu, C., and X. Yang, 1998. Study of remote sensing image texture analysis and classification using wavelet, *International Journal of Remote Sensing*, 13:3167-3187.